Springer

Journal of
Mechanical
Science and
Technology

Journal of Mechanical Science and Technology 22 (2008) 330~337

www.springerlink.com/content/1738-494x

# Effects of inlet blockage of gas-liquid scheme injector on acoustic tuning for acoustic damping in a combustion chamber

Chae Hoon Sohn* and I-Sun Park

*School of Mechanical and Aerospace Engineering, Sejong University, Seoul 143-747, Korea*

(Manuscript Received April 4, 2007; Revised November 3, 2007; Accepted November 5, 2007)

**Abstract**

In a rocket combustor, purely acoustic tuning of gas-liquid scheme injector is studied numerically for acoustic absorption by adopting linear acoustic analysis. Acoustic behavior in the combustor with a single injector is investigated to assure the optimum injector length. Acoustic-absorption effect of the injector is evaluated for cold condition by the quantitative parameter of damping factor as a function of injector length in the chamber for several boundary absorption coefficients. Irrespective of boundary absorption at the chamber wall, it is assured that the optimum tuning-length of the injector corresponds to half of a full wavelength of the first longitudinal overtone mode traveling in the injector with the acoustic frequency intended for damping in the chamber. Although boundary absorption affects little the tuning length of the injector, it appreciably affects damping capacity. Acoustic absorption at the wall increases with boundary absorption coefficient, but purely acoustic-damping effect induced by the tuned injector decreases with the coefficient. As another design parameter, effects of blockage at the injector inlet on acoustic tuning are investigated. It is found that the optimum injector length is shifted depending on the blockage ratio. Suitable combination of injector length and blockage should be made for maximum damping.

*Keywords*: Acoustic tuning; Gas-liquid scheme injector; Inlet blockage; Boundary absorption; Acoustic damping

## 1. Introduction

Acoustic instability is a phenomenon in which pressure oscillations are amplified through in-phase thermal interaction with combustion [1]. This may result in an intense pressure fluctuation as well as excessive heat transfer to combustor walls in systems such as solid and liquid propellant rocket engines, ramjets, turbojet thrust augmentors, utility boilers, and furnaces [2]. Although this has caused common problems in these systems, it has been reported that it occurs most severely in liquid rocket engines due to their high energy density. Thermal damage on the injector faceplate and combustor wall, severe mechanical vibration of the rocket body, and unpredictable malfunction of engines, etc., are the usual problems caused by acoustic instability. To understand this phenomenon, many studies have been conducted [1, 3-5], but it is still being pursued.

To suppress pressure oscillations, several methods can be adopted [3, 6]. One of them is passive control, which is to attenuate acoustic oscillation using combustion stabilization devices such as baffles, acoustic resonators, and acoustic liners. For example, an acoustic resonator can damp out or absorb pressure wave oscillating in the chamber using a well-tuned cavity [6, 7]. However, the devices are installed additionally and inevitably to suppress undesirable acoustic oscillations if they should be. And thus, negative effects of engine-performance degradation and complexity in engine manufacture accompany the installation of these devices.

On the other hand, in liquid rocket engines, injec-

*Corresponding author. Tel.: +82 2 3408 3788, Fax.: +82 2 3408 4333
E-mail address: chsohn@sejong.ac.kr
DOI 10.1007/s12206-007-1101-y

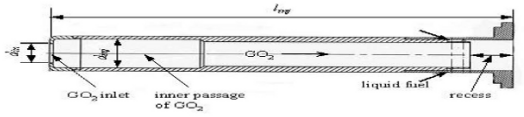


Fig. 1. Geometry of the coaxial gas-liquid scheme injector.

tors are mounted necessarily to the faceplate in order to inject propellants into the chamber. Depending on the phase of the injected propellants, they are classified into liquid-liquid scheme and gas-liquid scheme injectors. In high-performance the pump-fed liquid rocket engines, a staged combustion cycle is usually employed, where a preburner is used and regenerative cooling is adopted for the cooling of combustor wall [8]. In this system, the coaxial and gas-liquid scheme injector is typically used, which is illustrated in Fig. 1. As shown in this figure, gaseous oxidizer ($GO_2$) flows through the inner passage of the injector and then is mixed with liquid hydrocarbon fuel injected through several peripheral holes and, finally, both $GO_2$ and liquid fuel are injected into the chamber [9]. At this point, with the inside volume of the injector occupied by gas, it is noteworthy that the gas-liquid scheme injector can play a significant role in acoustic damping like acoustic resonators or damper in addition to its original function of propellant injection. Our previous works [10, 11] reported that the injector could function as a resonator and acoustic tuning of the injector would attenuate pressure oscillation to a good degree.

In this regard, acoustic tuning of the gas-liquid scheme injector is investigated intensively in this work. To a first approximation, only acoustic tuning is studied. In the previous works [10, 11], optimum injector length was investigated experimentally and numerically by adopting linear acoustic test and analysis, respectively. There are various design parameters for acoustic tuning of the injector. In this study, especially, effects of boundary absorption at the chamber wall and blockage at the injector inlet are emphasized for optimal acoustic tuning of the injector. For this, acoustic behaviors in the chamber with a single injector are investigated numerically by adopting linear acoustic analysis.

## 2. Numerical methods

### *2.1 Governing equation and solution method*

The acoustic field in a chamber can be calculated

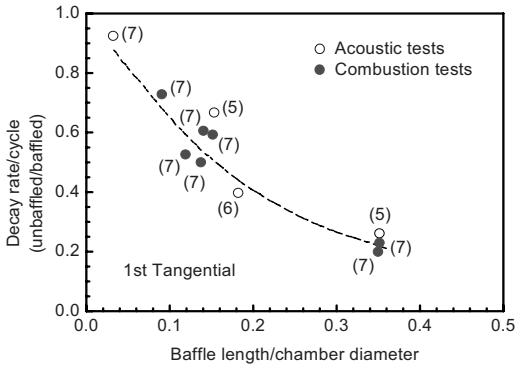


Fig. 2. Comparison of acoustic-test results with combustion-test results with respect to acoustic damping in a chamber (The number in parenthesis indicates the number of baffle blades [1]).

by solving a wave equation [12]. In the present study, purely acoustic behavior without mean flow is studied and combustion processes are not considered. The assumption of quiescent medium can be justified by the fact that mean flow affects resonant frequencies of transverse acoustic modes only by a factor of $\sqrt{1-\mathbf{M}^2}$, where $\boldsymbol{M}$ is the mach number of the mean flow [13]. Especially, tangential acoustic modes are little affected by the mean flow in the usual range of $\boldsymbol{M}$ (= 0.1~0.2) in a rocket combustion chamber. These effects of the mean flow have been investigated intensively in the previous work [14] as well. On the other hand, the previous work [15] showed that temperature distribution in a combustion chamber did not change fundamental aspects of acoustic behavior, and a good agreement between acoustic and combustion tests was reported in the previous works [1, 6]. One representative result is demonstrated in Fig. 2. The decay rate/cycle is a quantitative parameter for quantifying the capacity of combustion stabilization devices such as baffles and resonators. This encourages the adoption of purely acoustic models as reasonably accurate approximations of combustion acoustics when acoustic tuning of resonators or baffles is investigated.

For a homogeneous and non-dissipative medium, the linear wave equation can be derived as [12, 16]

$$\nabla^2 p' - \frac{1}{c_0^2}\frac{\partial^2 p'}{\partial t^2} = 0 \tag{1}$$

where $p'$ denotes pressure fluctuation, $c_0$ sound speed in the medium, and $t$ time. All acoustic variables are assumed to be temporally periodic for a given fre-

quency, *f*. With this harmonic assumption, unsteady solution in time domain can be transformed to steady solution in spectral domain, and thus, time-varying pressure fluctuation of $p'(\mathbf{x}, t)$ is expressed by complex acoustic pressure, $\widetilde{P}(\mathrm{x})$ in the form,

$$p'(\mathbf{x},t) = \mathrm{Re}\{\widetilde{p}'(\mathbf{x},t)\} = \mathrm{Re}\{\widetilde{P}(\mathbf{x})e^{-i\omega t}\} \tag{2}$$

where **x** denotes spatial coordinate vector, tilde (˜) complex variable, Re real part of complex variable, and $\omega = 2\pi f$ angular frequency. Through the transformation, the wave equation leads to the well-known Helmholtz equation,

$$\frac{\partial^2 \widetilde{P}}{\partial x^2} + \frac{\partial^2 \widetilde{P}}{\partial y^2} + \frac{\partial^2 \widetilde{P}}{\partial z^2} + k^2 \widetilde{P} = 0 \tag{3}$$

where *k* denotes wave number defined as $\omega$ divided by sound speed.

A harmonic analysis with Eq. (3) makes the problem much easier than solving the original unsteady wave equation, Eq. (1). To solve Eq. (3), an in-house FEM (Finite Element Method) code named KAA3D [17] is employed here. Eq. (3) is discretized in space by Galerkin's procedure [18] with the identical linear weighting and test functions on four-type hybrid elements (hexahedral, tetrahedral, prism, and pyramid). To deal with complex geometry, computational mesh can be generated by either an expert user-made grid generator or commercial software (e.g., GAMBIT, Fluent corporation) with a transformation of grid connectivity to be appropriate for KAA3D code. With the number of grid points, $N_p$, the $N_p \times N_p$ discretized equation set consists of real and imaginary parts and is transformed to a $2N_p \times 2N_p$ real system through equivalent real formulation. To enhance convergence and effectiveness for a large number of grid points (especially, $N_p$ greater than 30,000), the resultant sparse matrix is solved by using the GMRES (Generalized Minimal Residual) iterative technique with ILUT (Incomplete LU factorization with dual truncation strategy) preconditioner [19].

In previous works [17, 20], it was reported that the acoustic results calculated by KAA3D showed a good agreement with analytic and experimental data, and it has been used successfully for design of combustion stabilization devices. More details on numerical methods and calculation procedures adopted in KAA3D can be found in the literature [17, 20].

### *2.2 Numerical procedures*

Numerical procedures are quite similar to the acoustic experimental tests [6, 7, 10, 21]. Acoustic excitation is numerically imposed from a sound source, which corresponds to a loudspeaker, located on the faceplate near the chamber wall. The acoustic-pressure response is monitored by acoustic amplitude at the monitoring point, where a clear response is made. The monitoring point is located on the faceplate near the chamber wall at the opposite side to the sound source as shown in Fig. 3. Sine-wave acoustic oscillation is generated numerically by the sound source at the acoustic excitation point with arbitrary acoustic amplitude of 10 Pa and the acoustic frequency sweeping from 300 to 1,000 Hz for cold condition. By doing so, we obtain the acoustic response of the fluid within the chamber as a function of the frequency of acoustic excitation.

Pressure oscillation is absorbed by the solid wall because it is dissipated and its absorption depends on material property of the wall. In this study, acoustic absorption at the wall is adjusted by the boundary absorption coefficient specified at the wall [22]. That is, as a boundary condition at the wall, boundary absorption coefficients, $\beta$, of 0.002~0.008 are adopted. The coefficient values are estimated based on the previous experiments [21, 23], and they are typical values applicable for metal and acrylic material. When $\beta$ equals zero, there is no boundary absorption of sound waves at the wall. This indicates that the

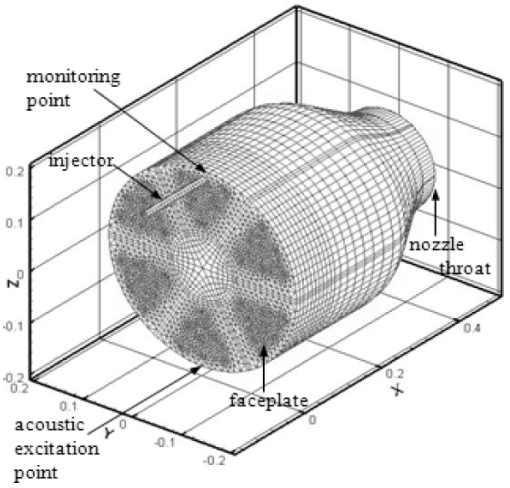


Fig. 3. Geometry and computational grids of the chamber with a single injector.

acoustic amplitude becomes infinitely large at any resonant modes of the chamber. With a certain value of $\beta$, acoustic resonant oscillation is damped and its amplitude becomes finite. On the other hand, the gas-liquid scheme injector has an open end at its inlet. The boundary condition at the inlet is enforced numerically to be an acoustically open boundary condition of $p' = 0$ $(\beta = \infty)$.

### *2.3 Combustion chamber and injector*

The geometry and computational grids of the chamber for the numerical analysis are shown in Fig. 3, which are the same as those adopted in the previous experimental and numerical works [10, 11]. The chamber domain ranges from the injector faceplate to the nozzle throat including the injector itself. The nozzle expansion part downstream of the throat is not considered since the part does not affect the acoustic field within the chamber. The sample chamber has the typical geometry of a liquid rocket combustion chamber. The diameters of the chamber and the nozzle throat, $D_{ch}$ and $D_{th}$, are 380 and 190 mm, respectively. The lengths from the faceplate to nozzle entrance and the throat, $L_e$ and $L_{th}$, are 250 and 478 mm, respectively and a half contraction angle in the conical section is 30°. It is assumed that the injector has complete cylindrical shape with the length of $l_{inj}$ and the blockage ratio of $B$ at $GO_2$ inlet. Besides, it is assumed that the injector has no recess for simplicity and clarity of acoustic investigation. Furthermore, injectors may generate and modify flow oscillations in them [24], but this is not considered here. The nondimensional parameter of blockage ratio, $B$, denotes the ratio of the blocked area to the injector cross-sectional area at gas ($GO_2$) inlet. In this study, with the diameter of the injector, $d_{inj}$ = 14 mm fixed, the injector length, $l_{inj}$ and the blockage ratio, $B$, are selected as the critical parameters for acoustic tuning and, thus, acoustic fields are calculated with variable parameters of $l_{inj}$ and $B$. The chamber wall and the faceplate have a wall boundary condition. When $B$ is not equal to zero, the wall boundary condition is also applied to the blocked or closed part at the inlet. The medium is assumed to be a quiescent air of which density, $\rho_0$, and sound speed, $c_0$, are 1.2 kg/m$^3$ and 340 m/s at 20 °C, respectively, for cold condition.

## 3. Results and discussions

### *3.1 Validation of the injector's role as a half-wave resonator and effects of boundary absorption*

In the chamber with a single injector, acoustic analyses are conducted with a variable injector length, $l_{inj}$ of 0 to 700 mm for several boundary absorption coefficients. Acoustic-pressure responses at the monitoring point are calculated as a function of the excitation frequency and are shown in Fig. 4 with the emphasis on the two lowest resonant modes of the chamber. As shown in this figure, irrespective of $\beta$, two peak responses occur at 414 and 548 Hz in the chamber without injector, i.e., $l_{inj}$ = 0. Judging from spatial distribution of acoustic pressure (acoustic field) at each mode, the first and second peaks have been identified as the 1st longitudinal (1L) and the 1st tangential (1T) modes, respectively. As $\beta$ increases, the amplitude of each peak decreases due to more acoustic absorption or damping at the wall for higher $\beta$.

Based on the calculated acoustic-pressure re-

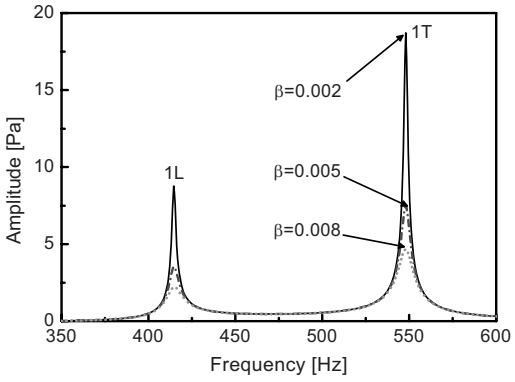


Fig. 4. Acoustic-pressure responses in a chamber without injector ($l_{inj}$ = 0) for several boundary absorption coefficients, $\beta$.

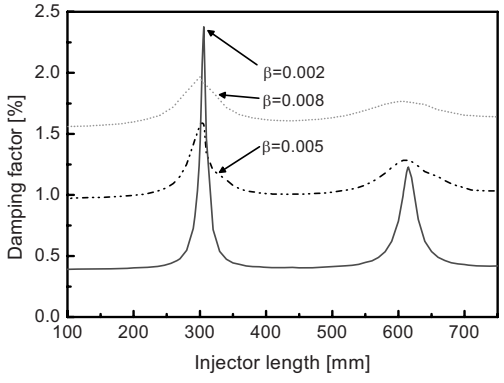


Fig. 5. Damping factors at 1T mode as a function of injector length for several boundary absorption coefficients, $\beta$.

sponses of the first tangential (1T) mode, damping factors, $\eta$ [6, 10, 11] are obtained for several $\beta$ and are shown as a function of $l_{inj}$ in Fig. 5. Higher damping factor indicates weaker acoustic oscillation or resonance. Accordingly, an acoustic resonator is more effective when a higher damping factor is obtained by the resonator. As $l_{inj}$ increases from 0, the damping factor increases gradually and, then, does so rapidly near $l_{inj}$ = 300 mm. As $l_{inj}$ increases further, the damping factor decreases rapidly and, then, a similar cyclic pattern is repeated. This pattern is observed irrespective of $\beta$. With $f_{1T}$= 548 Hz, which is of interest in this work, the wavelength ($\lambda$) of the 1st longitudinal overtone mode travelling inside the injector is calculated to be 620 mm.

When the injector functions as a half-wave resonator, the optimum length of the injector for maximum acoustic absorption has been derived theoretically as

$$l_{inj} = \frac{c_{inj}}{2f_0} - \Delta l \tag{4}$$

where $l_{inj}$ and $c_{inj}$ denote the injector length and sound speed of the fluid in the injector, respectively [11]. $\Delta l$ denotes length correction factor. This equation expresses theoretically the optimum length of the injector suppressing the acoustic oscillation coming from the chamber with the frequency of $f_0$. In Fig. 5, two peaks of $\eta$ occur at $l_{inj}$ = 303 ± 2 and 611 ± 4 mm. Accordingly, these are optimal tuning lengths and they correspond to a half wavelength, (1/2)$\lambda$ and a full wavelength, $\lambda$, respectively. Figure 5 shows that the injector can play a significant role as a half-wave resonator in acoustic damping or absorption of the tuned frequency oscillation (1T). The injector's role as a half-wave resonator and these acoustic behaviors except effects of $\beta$ can be verified by a comparison with experimental results reported in the previous work [10]. For example, with respect to tuning frequency and optimum length of the injector, the errors between numerical and experimental results are less than 2%. Although not shown here, the acoustic resonant frequencies, $f_{1L}$ and $f_{1T}$, have been rarely affected by single-injector installation and its length, but the acoustic amplitude of 1T mode has been affected appreciably by them. This also ensures that the injector can play a significant role in acoustic damping or absorption when it is tuned to the specific frequency as reported in the literature [10, 11].

As shown in Fig. 5, the boundary absorption has little contribution to modifying the tuning length of the injector. And when the injector is mal-tuned (i.e., $l_{inj}$ is far away from (1/2)$\lambda$), the damping factor increases with $\beta$. But, when the injector has optimal tuning length of 300 mm or so, $\beta$ = 0.002 produces the highest damping factor. This point can be explained as follows. Pressure oscillation in the chamber can be damped or absorbed by two factors: boundary absorption at the wall and acoustic absorption by the injector or resonator. Results shown in Fig. 5 indicate that with higher boundary absorption of the chamber wall, pressure oscillation is absorbed more effectively by the wall boundary rather than by the injector. In other words, the acoustic effect of the injector on acoustic absorption is dominant over boundary absorption at low $\beta$. This is demonstrated more clearly in Fig. 6, which shows damping factors in the chamber (a) without the injector, (b) with the optimally tuned injector of $l_{inj}$ = (1/2)$\lambda$, and (c) the difference of damping factor between the former and the latter, i.e., $\eta_{(b)} - \eta_{(a)}$. The first indicates acoustic damping induced by purely boundary absorption at the wall, the second by combined damping effect of the boundary absorption and the injector, and the third does acoustic damping induced by purely acoustic damping effect of the injector. From Fig. 6, the acoustic effect or the role of the injector as an acoustic resonator decreases appreciably with $\beta$. Furthermore, it is noteworthy that there exists a boundary absorption coefficient minimizing damping factor. Accordingly, an increase in $\beta$ is not always desirable when a resonator is installed for acoustic damping.

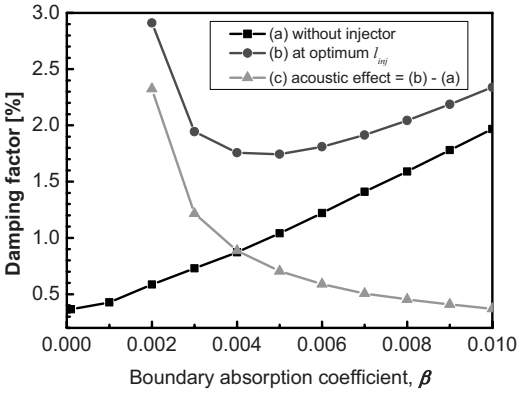


Fig. 6. Damping factors as a function of $\beta$ in a chamber (a) without injector, (b) with an injector of optimum length, and (c) $\eta(b) - \eta(a)$.

### *3.2 Effect of blockage on acoustic tuning of injector*

Another design parameter for acoustic tuning of the gas-liquid scheme injector may be the blockage ratio, $B$ at gas-propellant ($GO_2$) inlet. For similarity, we introduce a nondimensional parameter of inlet diameter, $d_{in}$ normalized by the inner diameter of the injector, $d_{inj}$ as shown in Fig. 1 and thereby, the normalized parameter of blockage ratio is defined as

$$B = \frac{d_{inj}^2 - d_{in}^2}{d_{inj}^2} \tag{5}$$

which denotes the ratio of the blocked area to the injector cross-sectional area.

Acoustic-pressure responses are calculated over a wide range of $B$ in the chamber of $\beta$ = 0.002 with a single injector of $l_{inj}$ = 304.5 mm = (1/2)$\lambda$, i.e., optimum injector length. From the numerical data, damping factor ratios defined as $\eta_B/\eta_{B=0\%}$, i.e., the ratio of $\eta$ at arbitrary value of $B$ to $\eta$ at $B$ = 0 %, are calculated and shown as a function of $B$ in Fig. 7(a). The damping factor maintains a nearly constant value at low blockage ratio and then decreases rapidly at high blockage ratio over 40 %. Its maximum is observed at $B$ = 0 %. This implies that blockage ratio can modify the optimum tuning length of the injector through variation of boundary condition at the injector inlet. Fig. 7(b) shows longitudinal profiles of pressure-fluctuation amplitudes inside the injector of $l_{inj}$ = (1/2)$\lambda$ for several blockage ratios. As discussed in the previous work [11], higher amplitude indicates that the injector is resonated or tuned more finely and it can absorb acoustic oscillation in the chamber more effectively. As shown in Fig. 7(b), the amplitude at $B$ = 0 % is the highest and this point is in a good agreement with the highest $\eta$ at $B$ = 0 % in Fig. 7(a).

With the slightly mal-tuned injector with $l_{inj}$ = 300 mm ≠ (1/2)$\lambda$, damping factor ratios are calculated and shown in Fig. 8. As $B$ increases, the damping factor increases and then decreases rapidly. The optimal blockage ratio can be found near 80%, which is distinct behavior from one shown in Fig. 7. This shows that the injector length and the blockage are closely coupled with each other for acoustic tuning of the injector. This is because the acoustic oscillation inside the injector is affected by the boundary condition at the injector inlet, which is changed by the blockage ratio, as well as the injector length. Although not

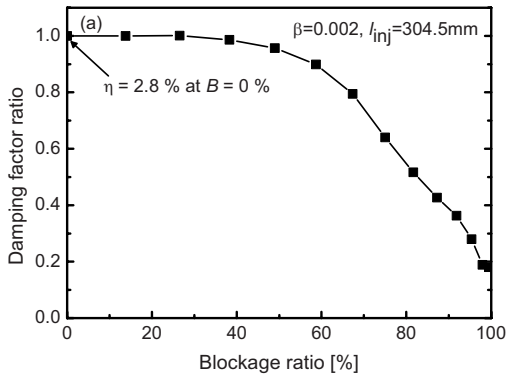


(a)

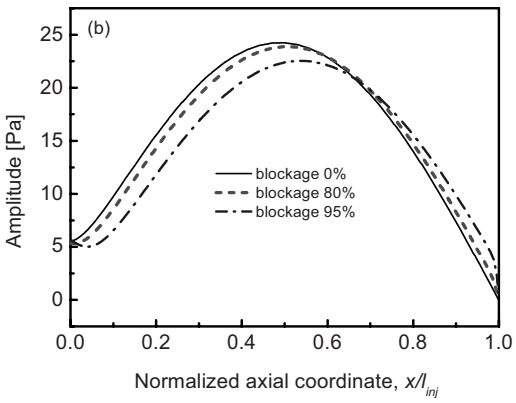


(b)

Fig. 7. Damping factor ratios as a function of blockage ratio in the chamber of $\beta$ = 0.002 with a single injector of optimum length, $l_{inj}$ = (1/2)$\lambda$ (a) and longitudinal profiles of pressure-fluctuation amplitudes inside the injector for several blockage ratios (b).

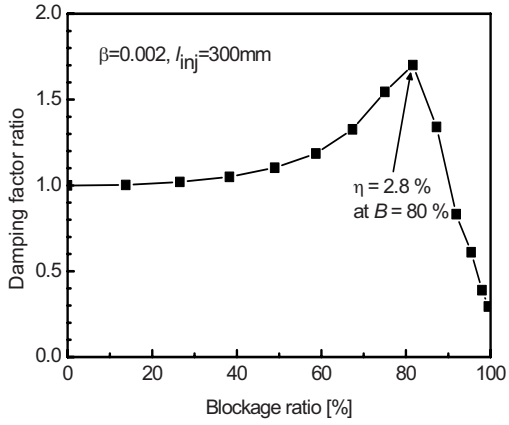


Fig. 8. Damping factor ratios as a function of blockage ratio in the chamber of $\beta$ = 0.002 with a single injector of non-optimum length, $l_{inj}$ ≠ (1/2)$\lambda$.

shown here, in the case of $l_{inj}$ = 300 mm, it is found that pressure-fluctuation amplitude inside the injector has its maximum near $B$ = 80 %. In two cases of optimal and non-optimal injector lengths, maxima of damping factor are observed at $B$ = 0 % and 80 %, respectively. But, it is found that the maximum value of $\eta$ is all the same in both cases. That is, the results show not only $\eta_{\max} = \eta_{B=0\%}$ = 2.8 % for the optimal length but also $\eta_{\max} = \eta_{B=80\%}$ = 2.8 % for a non-optimal length of $l_{inj}$ = 300 mm. Figs. 7 and 8 imply that there exists an optimal combination of the two parameters of $l_{inj}$ and $B$ for acoustic tuning of the injector.

To investigate the effect of blockage ratio on injector tuning length, acoustic analyses are conducted as a function of $l_{inj}$ over a wide range of $B$, and the calculated data of damping factor is shown in Fig. 9. The numerical data below $B$ = 50 % is similar to that at $B$ = 60 % and not shown here. As $B$ increases, the optimal or tuning length of injector decreases. But, it is also noteworthy that the maximum of $\eta$ has almost the same value of 2.8 % irrespective of the blockage ratio. Based on the data in Fig. 9, the optimal injector length is demonstrated as a function of blockage ratio for several boundary absorption coefficients in Fig. 10. The optimal length maintains a nearly constant value and decreases gradually with blockage ratio up to 70 % and then decreases rapidly by further increase in blockage ratio.

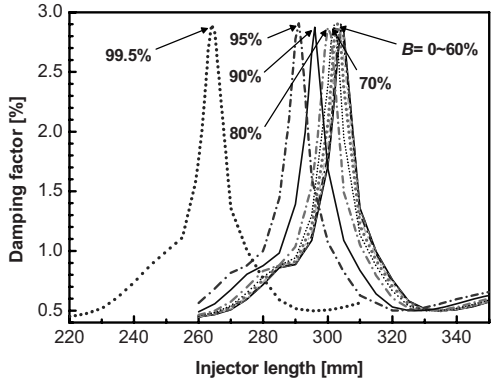


Fig. 9. Damping factors as a function of injector length over a wide range of blockage ratios.

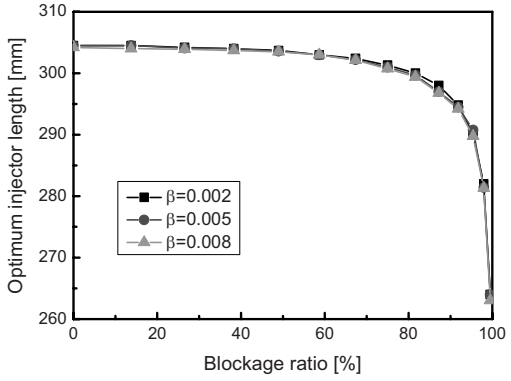


Fig. 10. Optimum injector lengths as a function of blockage ratio for several boundary absorption coefficients, $\beta$.

From Figs. 7-10, it is found that the injector tuned optimally at a wide-open inlet, i.e., $B$ = 0 %, does not play a role as a half-wave resonator at higher blockage ratio. And, it is noteworthy that constant damping capacity is maintained over the broad range of $B$ if the injector has the optimal length suitable for each $B$.

## 4. Concluding remarks

Acoustic-pressure responses in the chamber with gas-liquid scheme injector have been investigated numerically by adopting linear acoustic analysis. Acoustic behaviors in the chamber with a single injector have shown that the injector can absorb acoustic oscillation in the chamber most effectively when it has a tuning length of a half wavelength with respect to the acoustic frequency to be damped.

The boundary absorption affects little the tuning length of the injector. And when the injector is maltuned, the damping factor increases with boundary absorption coefficient, $\beta$. But, when the injector is optimally tuned, higher $\beta$ does not necessarily produce higher damping. Because the acoustic effect of the injector as a resonator or damper decreases appreciably with $\beta$, the damping factor shows nonlinear variation as a function of $\beta$ and has its minimum at the specific value of $\beta$. Accordingly, we should avoid the specific value of $\beta$ minimizing damping factor when the injector is designed as a resonator.

When we design the injector with the view of acoustic resonator, the blockage ratio at the gas-propellant ($GO_2$) inlet should be considered as an additional design parameter for acoustic tuning of the gas-liquid scheme injector. From acoustic analyses conducted over a wide range of blockage ratios, the blockage ratio affects the acoustics inside the injector and thereby shifts the optimal or tuning length of the injector. That is, although the injector is tuned optimally with respect to the length, i.e., $l_{inj} = (1/2)\lambda$, acoustic damping depends on the blockage at injector inlet as well. Numerical data shows that optimal in

jector length decreases with the blockage ratio. Accordingly, it is suggested that when the injector is designed as an acoustic resonator, the specific optimal length suitable for each blockage should be selected for maximum acoustic damping.

## References


[1] D. J. Harrje and F. H. Reardon (eds.), Liquid Propellant Rocket Combustion Instability, NASA SP-194, USA, (1972).

[2] K. R. McManus, T. Poinsot and S. M. Candel, A Review of Active Control of Combustion Instabilities, *Progress in Energy and Combustion Science* 19 (1993) 1-29.

[3] F. E. C. Culick and V. Yang, Liquid Rocket Engine Combustion Instability, Progress in Astronautics and Aeronautics, 169, AIAA, Washington DC, USA, (1995) 3-37.

[4] J. C. Oefelein and V. Yang, Comprehensive Review of Liquid-Propellant Combustion Instabilities in F-1 Engines, *Journal of Propulsion and Power* 9 (5) (1993) 657-677.

[5] S. Ducruix, T. Schuller, D. Durox and S. Candel, Combustion Dynamics and Instabilities: Elementary Coupling and Driving Mechanisms, *Journal of Propulsion and Power* 19 (5) (2003) 722-734.

[6] E. Laudien, R. Pongratz, R. Pierro and D. Preclik, Liquid Rocket Engine Combustion Instability, Progress in Astronautics and Aeronautics, 169, AIAA, Washington DC, USA, (1995) 377-399.

[7] R. B. Keller, Jr. (ed.), Liquid Rocket Engine Combustion Stabilization Devices, SP-8113, NASA, USA, (1974).

[8] D. K. Huzel and D. H. Huang, Modern Engineering for Design of Liquid-Propellant Rocket, Progress in Astronautics and Aeronautics, 147, AIAA, Washington DC, USA, (1992) 35.

[9] G. P. Sutton, History of Liquid-Propellant Rocket Engines in Russia, Formerly the Soviet Union, *Journal of Propulsion and Power* 19 (6) (2003) 1008-1037.

[10] H. Kim and C. H. Sohn, Experimental Study of the Role of Gas-Liquid Scheme Injector as an Acoustic Resonator in a Combustion Chamber, *Journal of Mechanical Science and Technology* 20 (6) (2006) 896-904.

[11] C. H. Sohn, I.-S. Park, S.-K. Kim and H. J. Kim, Acoustic Tuning of Gas-Liquid Scheme Injectors for Acoustic Damping in a Combustion Chamber of a Liquid Rocket Engine, *Journal of Sound and Vibration* 304 (2007) 793-810.

[12] M. J. Zucrow and J. D. Hoffman, Gas Dynamics, II, John Wiley & Sons, Inc., New York, USA, (1977) Chap. 15.

[13] M. S. Natanzon, Combustion Instability, Mashinostroyeniye, Moscow, Russia, (1986) Chap. 3.

[14] C. H. Sohn, I.-S. Park and S.-K. Kim, Effects of Mean Flow and Nozzle Damping on Acoustic Tuning of a Resonator in a Rocket Combustor, *Journal of the Korean Society of Propulsion Engineers* (in Korea). 10 (3) (2006) 41-47.

[15] C. H. Sohn and H. C. Cho, Numerical Analysis of Acoustic Characteristics in Gas Turbine Combustor with Spatial Non-homogeneity, *KSME International Journal* 18 (8) (2004) 1461-1469.

[16] T. Tsuji, T. Tsuchiya and Y. Kagawa, Finite Element and Boundary Element Modelling for the Acoustic Wave Transmission in Mean Flow Medium, *Journal of Sound and Vibration.* 255 (2002) 849-866.

[17] S.-K. Kim, H. J. Kim, W. S. Seol and C. H. Sohn, Acoustic Stability Analysis of Liquid Propellant Rocket Combustion Chambers, AIAA Paper 2004-4142. (2004).

[18] S. C. Chapra and R. P. Canale, Numerical Methods for Engineers, 2nd ed., McGraw-Hill, Singapore, (1989) Chap. 25.

[19] Y. Saad, SPARSKIT: a Basic Tool Kit for Sparse Matrix Computations, Ver. 2, Technical Report 90-20, Research Institute for Advanced Computer Science, NASA Ames Research Center, Moffet Field, CA, USA, (1990).

[20] S.-K. Kim, H. J. Kim and C. H. Sohn, Development of Analysis Code for Evaluation of Acoustic Stability of Rocket Engine Combustor with Various Designs, *Journal of The Korean Society for Aeronautical and Space Sciences* (in Korea). 32 (6) (2004) 110-116.

[21] Y. S. Ko, K. J. Lee and H. J. Kim, Acoustic Tests on Atmospheric Condition in a Liquid Rocket Engine Chamber, *Transactions of the KSME (B)* (in Korea). 28 (1) (2004) 16-23.

[22] L. E. Kinsler, A. R. Frey, A. B. Coppens and J. V. Sanders, Fundamentals of Acoustics, 4th ed., John Wiley & Sons, Inc., New York, USA, (2000) Chap. 2.

[23] C. H. Sohn, A Numerical Study on Acoustic Behavior in Baffled Combustion Chambers, *Transactions of the KSME (B)* (in Korea). 26 (7) (2002) 966-975.

[24] V. G. Bazarov and V. Yang, Liquid-Propellant Rocket Engine Injector Dynamics, *Journal of Propulsion and Power* 14 (5) (1998) 797-806.